

Suppressing the Skin–Core Structure of Injection-Molded Isotactic Polypropylene via Combination of an *in situ* Microfibrillar Network and an Interfacial Compatibilizer

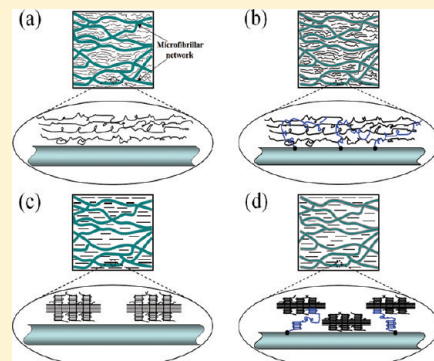
Xin Yi,[†] Chen Chen,[†] Gan-Ji Zhong,[†] Ling Xu,[†] Jian-Hua Tang,[‡] Xu Ji,[‡] Benjamin S. Hsiao,[§] and Zhong-Ming Li^{†,*}

[†]College of Polymer Science and Engineering and State Key Laboratory of Polymer Materials Engineering, Sichuan University, Chengdu 610065, P. R. China

[‡]School of Chemical Engineering, Sichuan University, Chengdu 610065, People's Republic of China

[§]Department of Chemistry, Stony Brook University, Stony Brook, New York 11794-3400, United States

ABSTRACT: Injection-molded semicrystalline polymer parts generally exhibited a so-called skin–core structure basically as a result of the large gradients of temperature, shear rate, stress, and pressure fields created by the boundary conditions of injection molding. Suppression of the skin–core structure is a long-term practical challenge. In the current work, the skin–core structure of the conventional injection-molded isotactic polypropylene (iPP) was largely relieved by the cooperative effects of an *in situ* microfibrillar network and interfacial compatibilizer. The *in situ* poly(ethylene terephthalate) microfibrils of 1–8 μm in diameter and large aspect ratios of above 40 tended to entangle with each other to generate a microfibrillar network in the iPP melt. During injection molding, the iPP molecules experienced confined flow in the microchannels or pores formed by the microfibrillar network, which could redistribute and homogenize the flow field of polymer melt. Addition of the compatibilizer, glycidyl methacrylate-grafted iPP, restrained the molecular orientation but facilitated preservation of oriented molecules due to the chemical bonds at the interface between PET microfibrils and iPP. The cooperative effects of *in situ* microfibrillar network and interfacial compatibilizer led to almost the same molecular orientation across the whole thickness of the injection-molded parts. Additionally, the content of β crystals in different layers of injection-molded iPP parts depended on the combined effects of the molecular orientation, the amount of oriented crystals, and the crystallization time between 105 and 140 °C. The presence of the interfacial compatibilizer facilitated formation of the β crystals because of preservation of the oriented molecules.



INTRODUCTION

Injection molding is one of the most common processing techniques for semicrystalline polymers, which enables an economical manufacturing of a large numbers of parts with complex geometry. However, injection molding production has its intrinsic disadvantages, for instance, the injection-molded parts usually exhibit an inhomogeneous structure, i.e., skin–core structure.^{1–7} The structural heterogeneity seriously deteriorates the mechanical properties of products due to the residual stress,^{8–10} and it may also cause poor surface quality and dimensional instability.¹¹ From a practical point of view, it is very necessary to eliminate the skin–core structure.

Skin–core structure formation of injection-molded parts has been extensively investigated, which is basically a result of the large gradients of temperature, shear rate, and stress fields created by the boundary conditions of injection molding.^{12–18}

During injection molding, the hot polymer melt fills the mold cavity quickly forced by a high injection pressure, the skin layer contacting mold walls experiences high strain, high stress, and a large cooling rate, and thus a high orientation is formed in this

area. While in the core region with weaker shear stress and a smaller cooling rate, the molecular chains have more time to relax and thus lead to a lower orientation. As a result, a distinct skin–core structure is formed in the injection-molded parts. However, to date, few works have been focused on restraining this inhomogeneous structure. Zhu et al. found that for the injection-molded polypropylene in the presence of a nucleating agent, the distribution of crystallinity and α -phase orientation index was independent of position through the sample depth, which indicated a nucleating agent likely suppresses the skin–core structure.^{19–21} In our previous work, we made full use of polymer microfibrils and a special injection-molding technology—shear-controlled orientation injection molding to suppress the skin–core structure of isotactic polypropylene (iPP).²² During injection molding, the microfibrils tended to entangle with each other to generate a microfibrillar network, which was able to

Received: December 13, 2010

Revised: April 12, 2011

Published: May 23, 2011

redistribute and homogenize the flow field of the polymer melt. Combining the effective nucleation effect of the polymer microfibrils and the continuous shear flow, the skin–core structure was completely eliminated. However, the effectiveness of this strategy depends on a special injection molding technology, which does not fit to the conventional injection molding. Besides, iPP and polymer microfibrils were not compatibilized, procuring an interface problem.

In order for more applications, in the current work, we attempted to focus on suppression of the skin–core structure of the conventional injection-molded polymer parts with the help of an in situ microfibrillar network and a compatibilizer. iPP was selected in our study for its good comprehensive properties and wide use as a commodity plastic.²³ The best candidate of the microfibrillar network is poly(ethylene terephthalate) (PET) since the PET microfibrillar network serves as a good heterogeneous nucleation agent for iPP.^{24,25} The glycidyl methacrylate-grafted iPP (iPP-g-GMA) was employed to improve the compatibility between the iPP and the PET microfibrillar network, whose epoxy groups can react with the hydroxyl ($-\text{OH}$) or carboxyl ($-\text{COOH}$) in PET chains.^{26–28}

EXPERIMENTAL SECTION

Material. The iPP (model HJ500) was supplied by Samsung Chemical Co., Korea, whose weight-average molecular weight (M_w), molecular weight distribution (M_w/M_n), and melt flow index (MFI) are 66.2×10^4 g/mol, 8.3, and 10 g/10 min (190 °C, 21.6 N), respectively. PET was a commercial bottle grade polyester, with the intrinsic viscosity $[\eta] = 0.658$ dL/g, supplied by Yi Zhen, China. The interface compatibilizer, PP-g-GMA, was prepared in our laboratory and reported in detail elsewhere.²⁹

Sample Preparation. The in situ PET microfibrils were prepared using the so-called “slit die extrusion-hot stretch-quenching” process.³⁰ The summarized procedures are as follows. First, melting of iPP and PET was completed by a single-screw extruder with the ratio of screw length to diameter, L/D , of 25. The temperature profile from hopper to die was 160, 270, 275, and 270 °C, and screw rotation was maintained at 80 rpm. Second, the melt passed through a slit die with 20 mm width and 1 mm thickness, then the extrudate was hot stretched by a take-up device with three pinching rolls, in which the volume flow rate of tap water was adjusted to keep the roll temperature. Finally, the stretched extrudate was immediately quenched in a cold water bath and then pelletized. The ratio of iPP to microfibrils is fixed at 85/15 by weight. The compatibilized iPP contained 8 wt % iPP-g-GMA based on the weight of iPP and microfibrils. Injection molding was performed on an injection molding machine (Nissin Co., Japan), and the temperature profile was set to 160, 205, 210, and 205 °C from hopper to nozzle, respectively, which is the processing temperature of iPP but far below the melting point of PET (about 265 °C).

Scanning Electronic Microscopy (SEM). For morphological observation of the microfibrillar network, the matrix iPP was partially etched away by hot xylene. After the solvent volatilized completely, the surfaces were coated with a layer of gold and observed in a JEOL JSM-5900LV SEM.

Differential Scanning Calorimetry (DSC). The thermal properties of the materials were determined on TA-DSC 910s with the following standard procedure: the samples with a weight of about 5–10 mg were melted at 200 °C for 5 min to eliminate

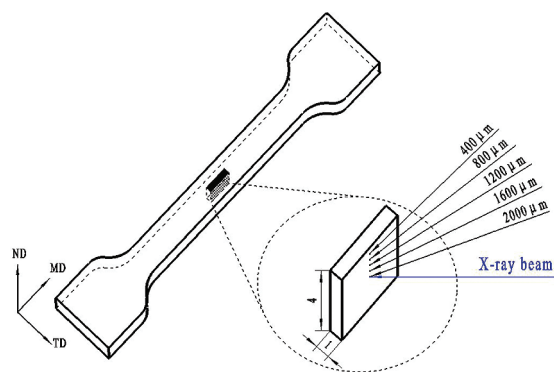


Figure 1. Schematic of the positions of samples for WAXS measurement; MD, the molding direction (i.e., flow direction), TD, the transverse direction, ND, the direction normal to the MD–TD plane. The numbers (400, 800, ..., 2000 in μm) represent the distance away from the sample surface along the ND direction.

the thermal history and then cooled to 30 °C at a constant rate of 10 °C/min under a nitrogen atmosphere. The dates were collected from 60 to 180 °C.

Dynamical Rheology Tests. The viscoelastic properties of iPP with and without a PET microfibrillar network were examined by a stress-controlled dynamic rheometer AR 2000ex (TA, USA) in a parallel-plate geometry. All samples were compressed into disks with a diameter of 25 mm and a thickness of 1 mm at 210 °C and 15 MPa. The strain and oscillation frequency range were 2.0% and 0.005–50 Hz, respectively.

Two-Dimensional Wide-Angle X-ray Diffraction (2D-WAXD) Measurement. The molecular orientation distributions and crystalline structure in the thickness direction were characterized by the two-dimensional wide-angle X-ray scattering (2D-WAXS), which was conducted at the X27C beamline in the National Synchrotron Light Source (NSLS), Brookhaven National Laboratory (BNL). The X-ray samples were machined from the 153.5 mm long, 10.2 mm wide, and 4.0 mm thick tensile bar to a 1 mm wide and 4.0 mm thick piece as shown in Figure 1, and the sample obtained is the middle section of the tensile bar. The direction normal to the MD–TD (the molding direction–transverse direction) plane was defined as ND, and the X-ray beam was perpendicular to the MD–ND plane and scanned five locations: 400, 800, 1200, 1600, and 2000 μm (center circle of the X-ray beam) down from the MD–TD surface. The wavelength of the monochromated X-ray from Cu K α radiation was 0.173 nm, and the distance from the sample to the detector was 68 mm. The diameter of the synchrotron illumination spot size was about 0.5 mm, and the samples were completely examined along the thickness. Two-dimensional WAXD images were collected with an X-ray CCD detector, which had a resolution of 1024 × 1024 pixels. Azimuthal scans (0–360°) of 2D-WAXS were made for the (040) crystal plane of iPP.

The orientation degrees of the crystal planes of iPP were calculated using Hermans' orientation parameter, which is defined as

$$f_H = (3\langle \cos^2 \phi \rangle - 1)/2 \quad (1)$$

where $\langle \cos 2\phi \rangle$ is an orientation factor defined as

$$\langle \cos^2 \phi \rangle = \int_0^{\pi/2} I(\phi) \cos^2 \phi \sin \phi \, d\phi / \int_0^{\pi/2} I(\phi) \sin \phi \, d\phi \quad (2)$$

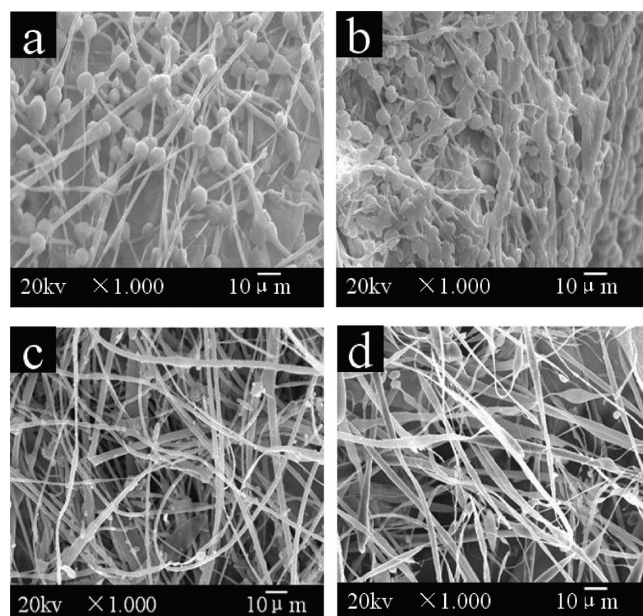


Figure 2. SEM images of the PET microfibrillar network with iPP matrix etching away by hot xylene at 110 °C for different times: (a and b) 60 and (c and d) 180 min (a and c) without compatibilizer and (b and d) with compatibilizer.

where $I(\phi)$ is the scattering intensity at ϕ , the angle between the normal of a given $(hk0)$ crystal plane and the shear flow direction. It is well known that the critical values of orientation parameters f_H indicate some special structure, such as, a value of $f_H = -0.5$ when all the c axes are perpendicular to the reference direction, a value of $f_H = 0$ with the mean of totally random orientation, and $f_H = 1.0$ for a perfect parallel orientation. In our research, the orientation parameter was calculated mathematically using Picken's method from the (040) reflection of WAXS for iPP.³¹

The 1D-WAXD profiles were obtained from circularly integrated intensities of 2D-WAXD image patterns, Gaussian functions were applied to fit the amorphous background, and an iterative peak-fit procedure was used to fit the crystalline reflections of WAXS profiles.

RESULTS

We first look into the existence of the in situ polymer microfibrillar network in iPP. To observe the original state of the microfibrils, we chose xylene to partially dissolve iPP. As shown in Figure 2, the interlocked microfibrillar network is visible, in which the microfibrils entangle with each other. The bare microfibrils are exposed after the iPP is completely etched away, which show 1–8 μm in diameter and large aspect ratios of above 40 (estimated by their diameter and visible length). A difference exists between the uncompatibilized and the compatibilized microfibrils. More ends are seen for the compatibilized microfibrils, which means a lower aspect ratio. The decrease of the aspect ratio is originated from an effective effect of the compatibilizer which can restrict transformation of dispersed phase particles into the fibrillar morphology.^{29,32} Interestingly, under the same etching conditions (temperature and time), the residual iPP sticking to the compatibilized microfibrils is much more than the uncompatibilized ones. This is reasonably ascribed

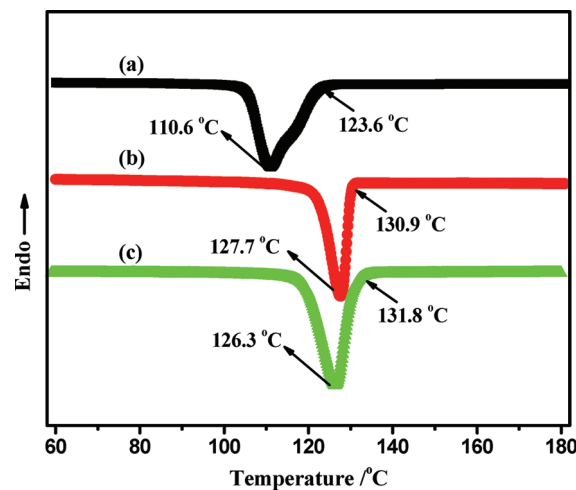


Figure 3. DSC cooling curves of (a) pure iPP, (b) iPP with a PET microfibrillar network, and (c) iPP with a compatibilized microfibrillar network.

to the good compatibilizing effect in the form of chemical bonding between PET chains and iPP-g-GMA.

Figure 3 shows DSC cooling curves of pure iPP and iPP with an uncompatibilized microfibrillar network and a compatibilized microfibrillar network. For pure iPP sample, the onset crystallization temperature (T_o) and peak crystallization temperature (T_p) are about 123.6 and 110.6 °C, respectively, while for the iPP with PET microfibrillar network, T_o and T_p are increased to around 130.9 and 127.7 °C (without compatibilizer) and 131.8 and 126.3 °C (with compatibilizer), respectively. At around 120 °C, the iPP with a PET microfibrillar network has almost finished crystallization whereas the neat iPP is just at the initial state of crystallization. These DSC results testify that the PET microfibrillar network can serve as a good heterogeneous nucleation agent for iPP. Furthermore, the nucleation effect becomes intense under flow conditions due to the shear-induced crystallization.³³ Additionally, a difference also exists between uncompatibilized and compatibilized samples with a microfibrillar network. The compatibilized one shows a lower crystallization rate than the one without compatibilizer, since the half-crystallization time for the compatibilized one is (about 28.9s) longer than the uncompatibilized iPP sample (about 20.2s). This discrepancy indicates that compatibilizer, iPP-g-GMA, in the microfibrillar network system weakens the heterogeneous nucleation.

The frequency dependence of the complex viscosity (η^*) for iPP with and without a microfibrillar network is shown in Figure 4. The solid-like microfibrillar network (nearly 55 °C below the PET melting point) increases the complex viscosity of the system remarkably, as testified elsewhere.³⁴ However, the case of a compatibilized system is completely different: the complex viscosity of this sample is almost the same as the pure iPP at the region of high frequency, which can be ascribed to a combination effect of the microfibrillar network and compatibilizer. Addition of compatibilizer tends to decrease the aspect ratio of PET microfibrils (see Figure 2), so the interlocked microfibrillar network has a relatively weaker effect on the increase of the complex viscosity. On the other hand, the compatibilizer itself has a lower molecular weight than pure iPP sample, so it not only improves the interfacial adhesion but also acts as a softening agent for iPP.³⁵ It should be pointed out that the complex

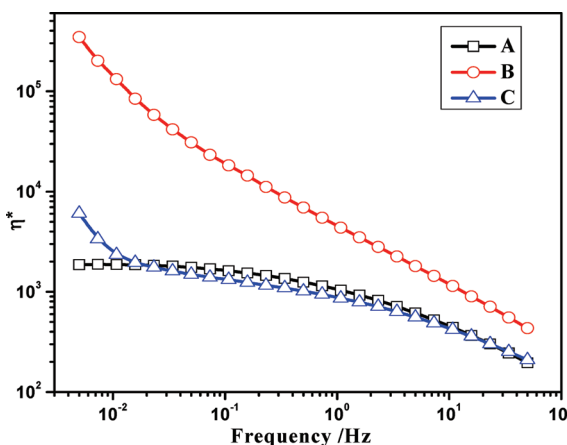


Figure 4. Dependence of complex viscosity on frequency at 210 °C: (A) pure iPP, (B) iPP with a PET microfibrillar network, and (C) iPP with a compatibilized microfibrillar network.

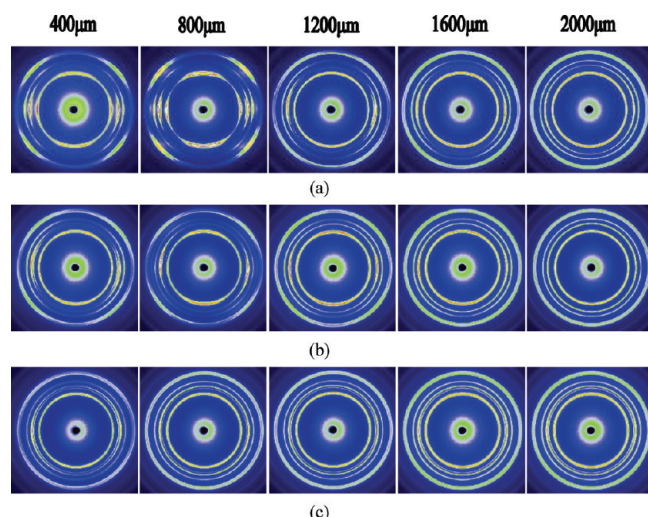


Figure 5. 2D-WAXS patterns of (a) pure iPP, (b) iPP with a PET microfibrillar network, and (c) iPP with a compatibilized PET microfibrillar network; the numbers, such as 400, 800, 1200, 1600, 2000 μm , mean the location down to the MD-TD plane.

viscosity of iPP with microfibrils is a result of a combination contribution of iPP and microfibrils, which indicates the truly apparent viscosity of iPP in the compatibilized sample is lower than the pure iPP under the same shear condition.

The next step is to evaluate whether the skin–core structure was successfully relieved, which was evaluated by 2D WAXS technology. Figure 5 shows the 2D-WAXS image patterns of iPP. The diffraction rings for the pure iPP sample exhibit a sharp contrast. There are varying arclike diffractions indicative of different molecular orientation in the outer layers, while no molecular orientation appears in the inner layer. This result indicates a typical skin–core structure in the pure iPP. For the sample with uncompatibilized microfibrils, like the pure iPP, there are still isotropic crystallites in the core layer and diffraction maximum in the outer layers; however, the arclike diffractions get wider, implying the difference of the molecular orientation diminishes. In contrast, the sample with compatibilized microfibrils assumes an un conspicuous skin–core structure across the

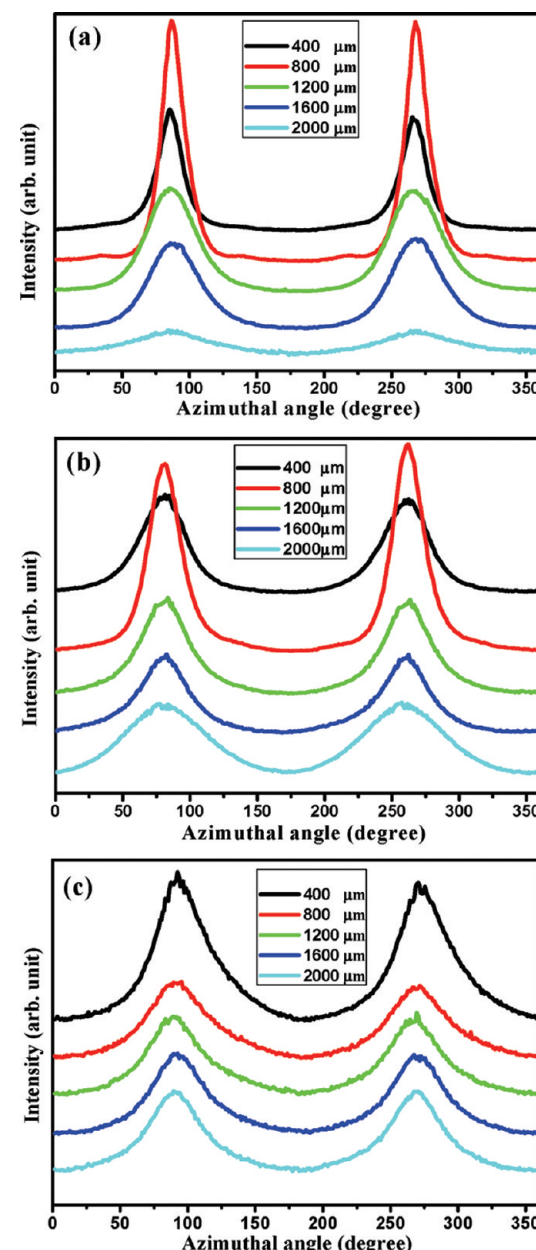


Figure 6. Intensity distribution of the (040) plane of the α crystal of iPP along the azimuthal angle for (a) pure iPP, (b) iPP with a PET microfibrillar network, and (c) iPP with a compatibilized PET microfibrillar network.

whole thickness of the sample, in which each layer shows very similar diffraction patterns.

To further evaluate the structure of injection-molded samples, the (040) intensity distribution along the azimuthal angle from 0 to 360° and the orientation parameter were estimated, as presented in Figures 6 and 7. The pure iPP sample shows a narrow and high diffraction intensity peak in the skin layer but almost no intensity maximum in the core layer, whose orientation parameter (f_H) is ca. 0.91 and 0.24, respectively, with a difference of 0.67. Apparently, a highly inhomogeneous structure exists in the neat iPP sample as observed in most conventional injection molding samples.^{36,37} The hierarchic structure was relieved to a degree for the sample with an uncompatibilized

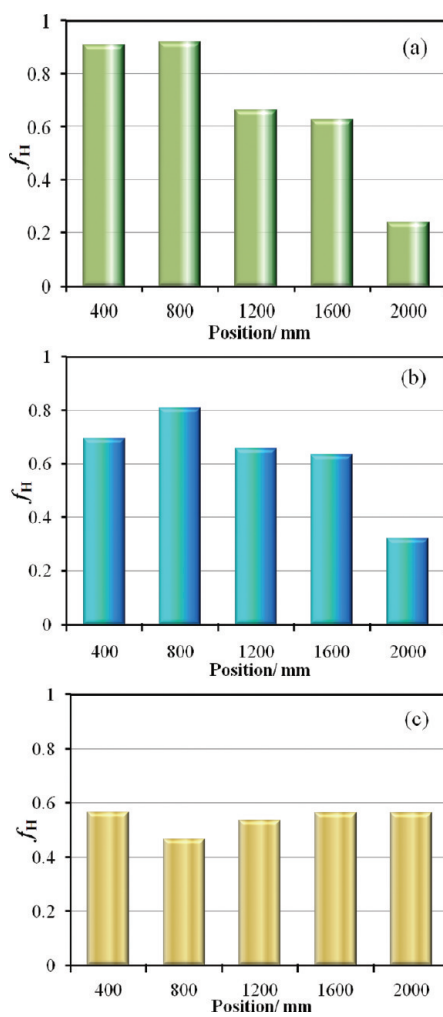


Figure 7. Orientation parameters of iPP, (a) pure iPP, (b) iPP with a PET microfibrillar network, and (c) iPP with a compatibilized microfibrillar network.

microfibrillar network. The diffraction intensity peaks are slightly similar to each other, whose orientation parameter stays between ca. 0.69 (skin) and 0.32 (core), with a reduced difference of orientation parameters, 0.37. More significantly, the sample with compatibilized microfibrils exhibits a nonhierarchic structure whose azimuthal intensity curves are very similar, and the orientation parameter along the thickness is around 0.56. These results indicate that the skin–core structure of the injection-molded iPP was greatly restrained with the help of an *in situ* polymer microfibrillar network and an interfacial compatibilizer.

Re-examining the 2D diffraction patterns in Figure 5, puny diffraction rings indicative of β -phase crystalline planes at $2\theta = 14.3^\circ$ (300) and 18.9° (311) are observed apart from the obvious diffraction rings representing five characteristic planes of α -phase crystals. The 1D-WAXD curves based on the diffraction peak position and integrated peak intensities can more vividly depict this phenomenon as shown in Figure 8. The diffraction peak intensity of the (300) plane is weak in skin layer and almost no β -crystal reflection signal in intermediate and core layers of the uncompatibilized sample. Interestingly, in the compatibilized sample, the (300) reflection for the β -form is much stronger; furthermore, the β -crystal exists in both shear and core layers.

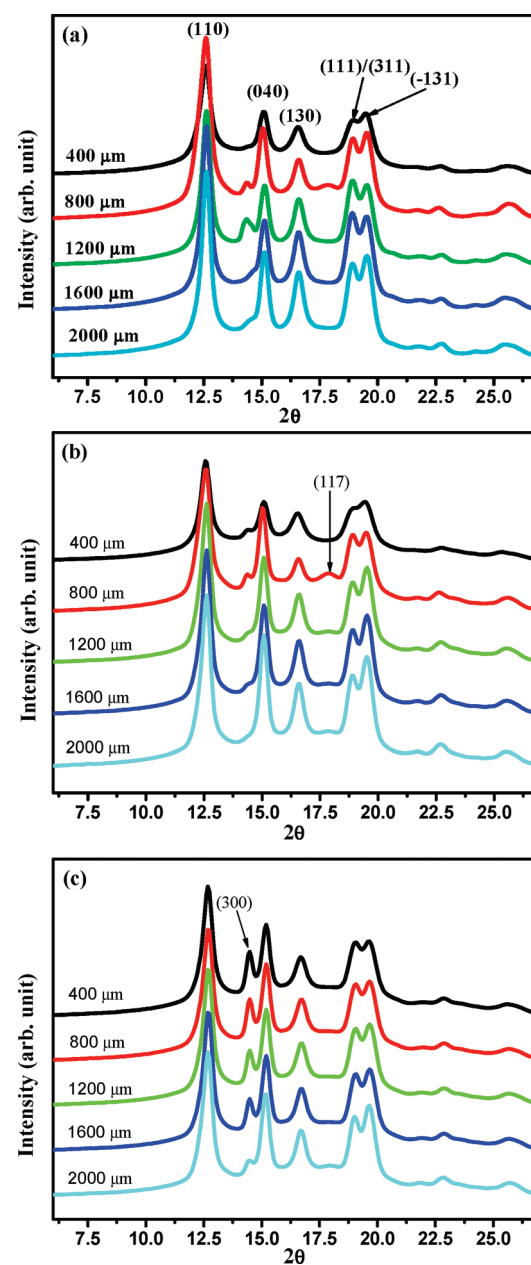


Figure 8. 1D-WAXS curves of (a) pure iPP, (b) iPP with a PET microfibrillar network, and (c) iPP with a compatibilized PET microfibrillar network at different locations obtained from circularly integrated intensities of 2D-WAXS patterns in Figure 5.

This trend shows that addition of compatibilizer, iPP-g-GMA, is in favor of formation of β -crystals.

■ DISCUSSION

The process of injection molding is very complex due to the thermomechanical history it experienced, such as high shear stress, shear strains, and pressures and complicated temperature gradients. For simplicity, it is always simulated by a flow-induced nonisothermal crystallization process for semicrystalline polymers, which was originally introduced by Janeschitz-Kreigl and co-workers,³⁸ but the essence of the crystallization process for semicrystal polymer in injection molding is far from clarity.^{39,40}

The shear flow occurring during mold filling may induce a transition from relatively isotropic, spherulitic crystals to highly oriented crystals, i.e., shish-kebabs morphology.⁴¹ The final molecular orientation of injection-molded parts is, though, a result of the competition between the shear-induced orientation and chain stretching and its subsequent relaxation. These generic rules take effect in the microstructure formation of the pure iPP samples in the present work. In the process of injection molding, the iPP melt with a high injection pressure was filled into the mold cavity accompanied by fountain flow at the flow front. The parts near the mold wall became sheared intensively due to the high flow rate of the melt and its friction with the wall, and it also solidified rapidly due to the cool mode wall, so a very thin unoriented layer (so-called surface layer) was formed.⁴¹ It should be noticed that this surface layer could not be examined by X-ray measurement alone in the present work due to the relatively large diameter of the synchrotron beam spot (about 0.5 mm), and this layer was neglected in the following discussion; meanwhile, the layer close to the surface layer was defined as the skin layer. Because of the very thin surface layer, the skin layer was also cooled down rapidly, and thus, the melt solidified rapidly by fast crystallization, during which the high orientation value of the skin layer of iPP was determined by the initial molecular orientation-dependent orientation, which was about 0.91. As the mold cavity was fully filled, the shear started to decay and the packing stage began. At this stage, due to low shear strains, the molecular orientation was also created due to further cooling.⁴² Then the solidification process of the core region was postponed corresponding to the skin layer due to the relatively poor heat conduction rate of the polymer, which meant there was enough time for initial stretched chains to relax in the interior region. Nevertheless, more or less oriented species were formed, giving rise to a certain degree of orientation. That is why the core layer of the pure iPP sample showed an orientation parameter of 0.23.

The case for the iPP sample with in situ polymer microfibrillar network is quite different. Under the same injection pressure as for the pure iPP, the iPP melt with a microfibrillar network had a lower flow rate to fill the mold due to the higher viscosity (see Figure 4). Thus, a lower shear rate was imposed on the skin layer, which decreased the orientation parameter (about 0.69) of the skin layer of the sample. In the core region, the situation was more complicated. On one hand, the iPP melt pushed the microfibrils into the mold, which led to some degree of preferred orientation of the microfibrils.²² The preferred orientation of the microfibrils triggered a relative movement (different velocity) and stress between the melt and the solid microfibrils. Thus, the microfibrillar network was effective as a solid wall and redistributed the flow field. The network split the space of the iPP melt movement, and hence, iPP molecules experienced confined flow in the microchannels or pores formed by the microfibrillar network. This scenario is schematically depicted in Figure 9a and 9b. Compared to the neat iPP melt, the local shear stress in the core region of the iPP melt with the microfibrillar network was high, which led to a higher orientation of molecular chains. On the other hand, the PET microfibrils served as an effective nucleation agent and nucleation enhancer under flow conditions, which increased both the onset temperature and the crystallization rate of the iPP (Figure 3).¹² The decrease of the crystallization time was in favor of the retention of orientated segments. The above two mechanisms led to a higher orientation (about 0.32) for the iPP sample with the uncompatibilized microfibrils in the

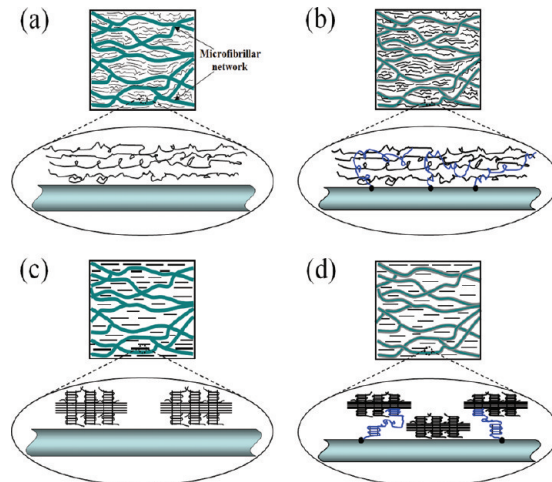


Figure 9. Structure models of uncompatibilized (a and c) and compatibilized (b and d) iPP with a microfibrillar network. Molecule structure of iPP in melting during injection molding (a and b) and in the final injection product (c and d). The black points represent the chemical bonds between PET and compatibilizer, iPP-g-GMA.

core region and consequently reduced the difference of the orientation parameter between the skin and the core.

For the iPP sample with a compatibilized microfibrillar network the most obvious feature is the presence of a homogeneous crystal orientation, rather than the obvious skin–core structure. The orientation degree of its skin layer was lower than the uncompatibilized parts, but it was the opposite in its core layer. This interesting feature is attributed to the presence of the compatibilizer, iPP-g-GMA, which performed combination effects of creating chemical bonds at the interface and reducing the melting viscosity of the blend with the PET microfibrils network. As mentioned above, during mold filling, the iPP melt pushed the microfibrillar network to move but baffled itself to flow. The compatibilizer reduced the complex viscosity, even lower than pure iPP, which meant easier molecule orientation during mold filling and packing and easier molecule relaxation simultaneously. Meanwhile it bridged the microfibrils and the iPP chains to make the molecular orientation harder and led to a lower orientation parameter (about 0.56) in the skin layer in comparison to the uncompatibilized one, as shown in Figure 9a. In theory, at the beginning of packing, a solidified outer layer (possibly including the very thin unoriented layer and skin layer or intermediate layer) had been formed due to the fast crystallization, but the thickness of this layer was different between the pure iPP sample and the iPP with PET microfibrils network due to the heterogeneous nucleation of PET microfibrils. The prominent nucleation effect made the outer layer solidify faster, and the thickness of the sample with a PET microfibrillar network became larger than pure iPP. Thickening of the outer layer reduced the cross-section through which the melt still flowed during packing.⁴¹ Comparing the iPP samples with and without compatibilizer, the low shear flow rate during packing was hardly enough to push the melt with increased shear stress and induced molecule orientation due to high viscosity in the uncompatibilized system, but the case in the compatibilized system was different, the low flow rate could still make melt flow even though the shear stresses increased during packing. This contributed to a relatively high molecule orientation parameter in the core layer of the compatibilized system with a PET microfibrillar network. Furthermore,

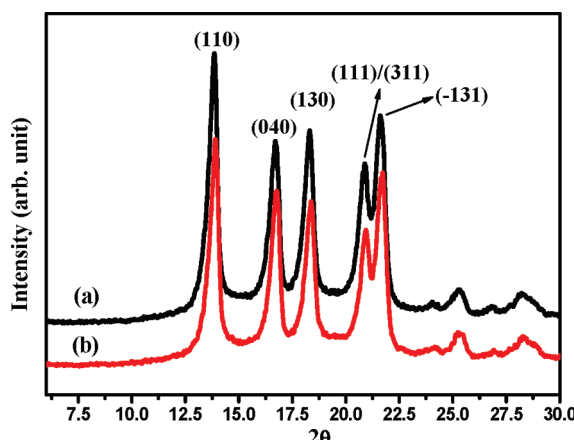


Figure 10. XRD curves of (a) neat iPP and (b) blend iPP/iPP-g-GMA with a weight ratio of 80/20.

because of the compatibilizer's restraint, the oriented iPP chains relaxed more slowly, thus preserving more molecular orientation as shown in Figure 9d. Thus, the core layer of the compatibilized sample reasonably had a higher orientation parameter (about 0.56). Here, a conclusion comes into being that the compatibilizer restrained the molecular orientation but facilitated preservation of oriented molecules (Figure 9b and 9d, which schematically illustrates the role of the interfacial compatibilizer). These two competitive effects together with the influence of the microfibrillar network greatly relieved the skin–core structure in the injection-molded iPP parts.

Compared to the iPP sample with the uncompatibilized microfibrillar network, the iPP sample with a compatibilized microfibrillar network formed an appreciable amount of β -modification crystals in skin, intermediate, as well as core layers. It seems the compatibilizer, iPP-g-GMA, induced formation of β -crystals. Unexpectedly, the additional experiment showed that, under quiescent condition, the iPP with a compatibilizer did not crystallize into any β -crystals (Figure 10), since obviously both of the samples exhibit the characteristic peak of the α -form crystal at 13.8° , 16.7° , 18.3° , 20.8° , and 13.8° corresponding to (110), (040), (130), (111), and (131), respectively.

The presence of β -crystals is therefore attributed to shear-induced orientation crystallization. The shear-induced β -crystal formation was first observed by Leugering, et al.⁴³ and later thoroughly studied by Varga,⁴⁴ Hsiao, An et al.^{45,46} A general opinion is held that shearing of the iPP melt would more likely form α -row nuclei and then a subsequent growth of the β -phase on the formed α -row nuclei; furthermore, only the iPP crystallization between $T_{\alpha\beta}$ (ca. 140°C) and $T_{\beta\alpha}$ (ca. 105°C) facilitates formation of β crystals.^{47,48} On this basis one can understand the content of β crystals of pure iPP in various layers. In the skin layer, the strong molecular orientation can induce a large amount of α -row nuclei, which provides the precondition of forming β crystals. However, the fast cooling rate in this area leaves a very short time for iPP melt staying between 105 and 140°C . Thus, it is hard to detect the reflection of β crystals in the skin layer. In contrast, in the intermediate region the relatively high molecular orientation and long crystallization time between 105 and 140°C make it possible to form a certain content of β crystals, while in the core region the weak shear stress and long time to relax the oriented molecules go against forming

α -row nuclei; thus, the β crystals are hardly developed. For the iPP sample with an uncompatibilized microfibrillar network, no β crystals appear, which is ascribed to the distinct α -phase heterogeneous nucleation of the PET microfibrillar network. Among neat iPP and iPP samples with the microfibrils, the iPP sample with an uncompatibilized microfibrillar network has the highest crystallization rate under the same conditions (Figure 3), which greatly shortened the time to form a β crystal between 105 and 140°C in the skin and intermediate layers. In the core layer, the low molecular orientation is still the major reason for no β crystal. The unexpected result appears in the sample with a compatibilized microfibrillar network that the β crystal exists not only in the intermediate layer but also in the skin and core regions. First, it is necessary to notice that the compatibilizer, iPP-g-GMA, suppressed the heterogeneous nucleation of PET microfibrils, which allows it to crystallize into β crystals for a longer time than the uncompatibilized sample, while in the core layer more oriented molecules were reserved, which is conducive to form more α -row nuclei and make it possible to form more β crystals. In conclusion, the content of the β crystal in different layers is dependent on the cooperative effect of the molecular orientation, relaxation of oriented molecules, and time staying between 105 to 140°C .

CONCLUSION

An attempt to tailor the conventional injection parts' skin–core structure was successfully accomplished using an in situ microfibrillar network and a compatibilizer. The microfibrillar network worked effectively as a solid wall and redistributed the flow field, since the network split the space of the iPP melt movement, and hence, iPP molecules experienced confined flow in the microchannels or pores in the microfibrillar network. In addition to the distinct heterogeneous nucleation of microfibrils, the "skin–core structure" was relieved by reducing the gap of the orientation parameters between the skin layer, the intermediate layer, and the core region. Furthermore, addition of compatibilizer can further homogenize the orientation distribution across the thickness direction of injection-molding samples, which is attributed to the combination of a PET microfibrillar network (effect of the heterogeneous nucleation and redistribution, homogenization of flow field) and compatibilizer (effect of reducing the complex viscosity of the matrix and maintaining oriented molecules during crystallization). Furthermore, β -form crystals can be formed in the iPP sample with a compatibilized PET microfibrillar network while almost not in an uncompatibilized one.

AUTHOR INFORMATION

Corresponding Author

*E-mail: zml@scu.edu.cn

ACKNOWLEDGMENT

The authors are indebted to Dr. Lixia Rong and Jie Zhu from the Synchrotron Light Source, Brookhaven National Laboratory, for their help with the WAXD measurements. The Chinese team is grateful for financial support of this subject by the National Natural Science Foundation of China (grant no. 20776087, 20876099), the National Programs for High Technology Research and Development of China (grant no. 2008AA03Z510),

and the National Outstanding Youth Foundation of China (grant no. 50925311).

■ REFERENCES

- (1) Warner, T. J.; Stobbs, W. M. *Acta Metall.* **1989**, *37*, 2873.
- (2) Dyer, S. R. A.; Lord, D.; Hutchinson, I. J.; Ward, I. M.; Duckett, R. A. *J. Phys. D* **1992**, *25*, 66.
- (3) Sayers, C. M. *Int. J. Solids Struct.* **1992**, *29*, 2933.
- (4) Kantz, M. R.; Newman, H. D.; Stigale, F. H. *J. Appl. Polym. Sci.* **1972**, *16*, 1249.
- (5) Trotignon, J. P.; Verdu, J. *J. Appl. Polym. Sci.* **1987**, *34*, 1.
- (6) Fujiyama, M.; Wakino, T.; Kawasaki, Y. *J. Appl. Polym. Sci.* **1988**, *35*, 29.
- (7) Mencik, Z.; Fitchmun, D. R. *J. Polym. Sci., Polym. Phys. Ed.* **1973**, *11*, 973.
- (8) Kubát, J.; Møanson, J. A.; Rigdahl, M. *Polym. Eng. Sci.* **1983**, *23*, 877.
- (9) Kalay, G.; Sousa, R. A.; Reis, R. L.; Cunha, A. M.; Bevis, M. J. *J. Appl. Polym. Sci.* **1999**, *73*, 2473.
- (10) Schrauwen, B. A. G.; Breemen, L. C. A.; Spoelstra, A. B.; Govaert, L. E.; Peters, G. W. M.; Meijer, H. E. H. *Macromolecules* **2004**, *37*, 8618.
- (11) Zuidema, H.; Peters, G. W. M.; Meijer, H. E. H. *Macromol. Theory Simul.* **2001**, *10*, 447.
- (12) Trotignon, J. P.; Lebrun, J. L.; Verdu, J. *Plast. Rubber Process Appl.* **1982**, *2*, 247.
- (13) Zipper, P.; Janosi, A.; Geymayer, W.; Ingolic, E.; Fleischmann, E. *Polym. Eng. Sci.* **1996**, *36*, 467.
- (14) Kalay, G.; Bevis, M. J. *J. Polym. Sci., Part B: Polym. Phys.* **1997**, *35*, 241.
- (15) Hsiung, C. M.; Cakmak, M. *J. Appl. Polym. Sci.* **1993**, *47*, 125–47.
- (16) Hsiung, C. M.; Cakmak, M. *J. Appl. Polym. Sci.* **1993**, *47*, 149–65.
- (17) Ulcer, Y.; Cakmak, M.; Miao, J.; Hsiung, C. M. *J. Appl. Polym. Sci.* **1996**, *60*, 669.
- (18) Ulcer, Y.; Cakmak, M. *Polymer* **1997**, *38*, 2907.
- (19) Zhu, P. W.; Edward, G. *Macromol. Mater. Eng.* **2003**, *288*, 301.
- (20) Zhu, P. W.; Phillips, A. A.; Edward, G. *J. Appl. Phys.* **2005**, *97*, 104908.
- (21) Zhu, P. W.; Tung, J.; Phillips, A. A.; Edward, G. *Macromolecules* **2006**, *39*, 1821.
- (22) Zhong, G. J.; Li, L. B.; Mendes, E.; Byelov, D.; Fu, Q.; Li, Z. M. *Macromolecules* **2006**, *39*, 6771.
- (23) Loos, J.; Schimanski, T.; Hofman, J.; Peijs, T.; Lemstra, P. *J. Polym.* **2001**, *42*, 3827–3834.
- (24) Li, Z. M.; Yang, Wei.; Li, L. B.; Xie, B. H.; Huang, R.; Yang, M. B.; Feng, J. M. *J. Polym. Sci., Part B: Polym. Phys.* **2004**, *42*, 374.
- (25) Wang, C.; Liu, C. R. *Polymer* **1999**, *40*, 289.
- (26) Jayanarayanan, K.; Thomas, S.; Joseph, K. *Composites, Part A* **2008**, *39*, 175.
- (27) Durgun, H.; Bayram, G. *J. Adhes. Sci. Technol.* **2005**, *19*, 407.
- (28) Cartier, H.; Hu, G. H. *J. Polym. Sci., Part A: Polym. Chem.* **1998**, *36*, 1053.
- (29) Yi, X.; Xu, L.; Wang, Y. L.; Zhong, G. J.; Ji, X.; Li, Z. M. *Eur. Polym. J.* **2010**, *46*, 719.
- (30) Li, Z. M.; Li, L. B.; Shen, K. Z.; Yang, W.; Huang, R.; Yang, M. B. *Macromol. Rapid Commun.* **2004**, *25*, 553.
- (31) Picken, S. J.; Aerts, J.; Visser, R.; Northolt, M. G. *Macromolecules* **1990**, *23*, 3849.
- (32) Fakirov, S.; Bhattacharyya, D.; Lin, R. J. T.; Fuchs, C.; Friedrich, K. *J. Macromol. Sci., Part B: Phys.* **2007**, *46*, 183.
- (33) Li, Z. M.; Li, L. B.; Shen, K. Z.; Yang, W.; Huang, R.; Yang, M. B. *Polymer* **2005**, *46*, 5358.
- (34) Xu, H. S.; Li, Z. M.; Pan, J. L.; Yang, W.; Yang, M. B. *Polym. Eng. Sci.* **2005**, *45*, 1231.
- (35) Friedrich, K.; Evstatiev, M.; Fakirov, S. *Compos. Sci. Technol.* **2005**, *65*, 107.
- (36) Yu, X. F.; Wu, H.; Li, J.; Guo, S. Y.; Qiu, J. H. *Polym. Eng. Sci.* **2009**, *49*, 703.
- (37) Cao, J.; Wang, K.; Cao, W.; Zhang, Q.; Du, R. N.; Fu, Q. *J. Appl. Polym. Sci.* **2009**, *112*, 1104.
- (38) Liedauer, S.; Eder, G.; Janeschitz-Kriegl, H.; Jerschow, P.; Geymayer, W.; Ingolic, E. *Int. Polym. Proc.* **1993**, *VIII*, 236.
- (39) Favaro, M. M.; Marinelli, A. L.; Farah, M.; Bretas, R. E. S. *Polym. Eng. Sci.* **2008**, *48*, 257.
- (40) Kim, K. H.; Isayev, A. L.; Kwon, K.; Sweden, C. *Polymer* **2005**, *46*, 4183.
- (41) Housmans, J. W.; Gahleitner, M.; Peters, G. W. M.; Meijer, H. E. H. *Polymer* **2009**, *50*, 2304.
- (42) Baaijens, F. P. T. *Rheol. Acta* **1991**, *30*, 284.
- (43) Leugering, H. J.; Kirsch, G. *Angew. Makromol. Chem.* **1973**, *33*, 17.
- (44) Varga, J.; Karger-Kocsis, J. *J. Polym. Sci., Part B: Polym. Phys.* **1996**, *34*, 657.
- (45) Somani, R. H.; Hsiao, B. S.; Nogales, A.; Fruitwala, H.; Srinivas, S.; Tsou, A. H. *Macromolecules* **2001**, *34*, 5902.
- (46) Huo, H.; Jiang, S. J.; An, L. J.; Feng, J. C. *Macromolecules* **2004**, *37*, 2478.
- (47) Somani, R. H.; Hsiao, B. S.; Nogales, A.; Fruitwala, H.; Srinivas, S.; Tsou, A. H. *Macromolecules* **2001**, *34*, 5902.
- (48) Kumaraswamy, G.; Korneld, J. A.; Yeh, F.; Hsiao, B. S. *Macromolecules* **2002**, *35*, 1762.